ISSN 0021-3640, JETP Letters, 2011, Vol. 94, No. 6, pp. 481–489. © Pleiades Publishing, Inc., 2011.
Original Russian Text © Yu.I. Latyshev, A.P. Orlov, 2011, published in Pis'ma v Zhurnal Eksperimental'noi i Teoreticheskoi Fiziki, 2011, Vol. 94, No. 6, pp. 517–526.

Quantum Coherent Effects in Layered Nanostructures

Yu. I. Latyshev and A. P. Orlov

Kotel'nikov Institute of Radio Engineering and Electronics, Russian Academy of Sciences, ul. Mokhovaya 11-7, Moscow, 125009 Russia

Received July 15, 2011

Magnetotransport in structures based on $NbSe_3$, $Bi_2Sr_2CaCu_2O_{8+x}$, and graphite has been examined. The stimulation of the charge density wave gap by a high magnetic field in $NbSe_3$ has been detected and studied using interlayer tunneling spectroscopy. It has been shown that this stimulation is of orbital character and the effect of the Zeeman splitting of the ground state of the charge density wave on this stimulation has been analyzed. The second harmonic of the gap singularity of the charge density wave in tunneling spectra, which is associated with the cascade relaxation of quasiparticles with the excess energy 2Δ. The effects caused by the interaction between Josephson vortices and Abrikosov vortex filaments have been studied on $Bi_2Sr_2CaCu_2O_{8+x}$ mesas. Studies of the magnetoresistance of thin graphite with nanoholes reveal a significant contribution to the magnetotransport from Dirac fermions and provide experimental evidence of the existence of edge states around nanoholes.

DOI: 10.1134/S002136401118007X

1. INTRODUCTION

This work is devoted to the study of coherent effects in materials with reduced size using various nanostructures. We study three classes of layered materials, including high-temperature superconductors ($Bi_2Sr_2CaCu_2O_{8+x}$), materials with a charge density wave ($NbSe_3$), and graphite. The most general investigations for all of these materials were associated with interlayer tunneling spectroscopy on mesa-type structures, where transport occurs across layers in the region of small lateral sizes. In addition, we studied structures containing nanoholes (column defects), including nanometer-thick graphite samples with thicknesses varying from a few dozen to just a few graphene layers. We discuss the experiments on the interlayer tunneling spectroscopy of a state with a charge density wave in $NbSe_3$, some new effects caused by the interlayer Josephson interaction in $Bi_2Sr_2CaCu_2O_{8+x}$, and quantum interference effects due to the contribution from Dirac fermions in thin graphite single crystals.

2. INTERLAYER TUNNELING SPECTROSCOPY OF $NbSe_3$

Using interlayer tunneling spectroscopy, we previously examined the temperature dependence of the charge density wave energy gap in $NbSe_3$ and *o*-TaS_3 [1, 2], studied the interaction between two charge density waves coexisting in $NbSe_3$ at low temperatures [3], and revealed intragap states in $NbSe_3$ [4, 5]. In recent experiments, which will be reported below, the spectroscopy of the charge density wave energy gap in $NbSe_3$ was used for measurements in high magnetic fields [6] in the temperature region of fluctuations of the charge density wave above the Peierls transition temperature [7] and the features of tunnel spectra in the energy region of the double energy gap were analyzed.

2.1. Spectroscopy of the Charge Density Wave Gap in $NbSe_3$ *in High Magnetic Fields*

The idea that a magnetic field can suppress pockets of the Fermi surface in which carriers that are not condensed in the charge density wave are localized was first proposed more than 25 years ago by Balseiro and Falicov [8] when they examined the experimental detection of the anomalously large magnetoresistance in $NbSe_3$ at low temperatures [9]. Gor'kov and Lebed [10] proposed the mechanism that explains this phenomenon by the fact that the magnetic field suppresses the motion of uncondensed carriers transverse to the wavevector of the charge density wave and makes it closer to uniform. Zanchi, Bjelis, and Montabaux [11] calculated the magnetic field dependence of the Peierls transition temperature. At small nesting imperfection parameters, the dependence exhibits an initial increase, a maximum, and then a decrease. In other words, the theory developed in [11] predicted the possibility of inducing a state with the charge density wave by the magnetic field above the Peierls transition temperature T_p. The effect is manifested at the field scale $H \approx kT_p/\mu_B$, where μ_B is the Bohr magneton. For $NbSe_3$ with $T_p = 59$ K, this field is about 60 T. We attempted to study this effect on $NbSe_3$ mesas using interlayer tunneling spectroscopy in pulsed magnetic fields [6].

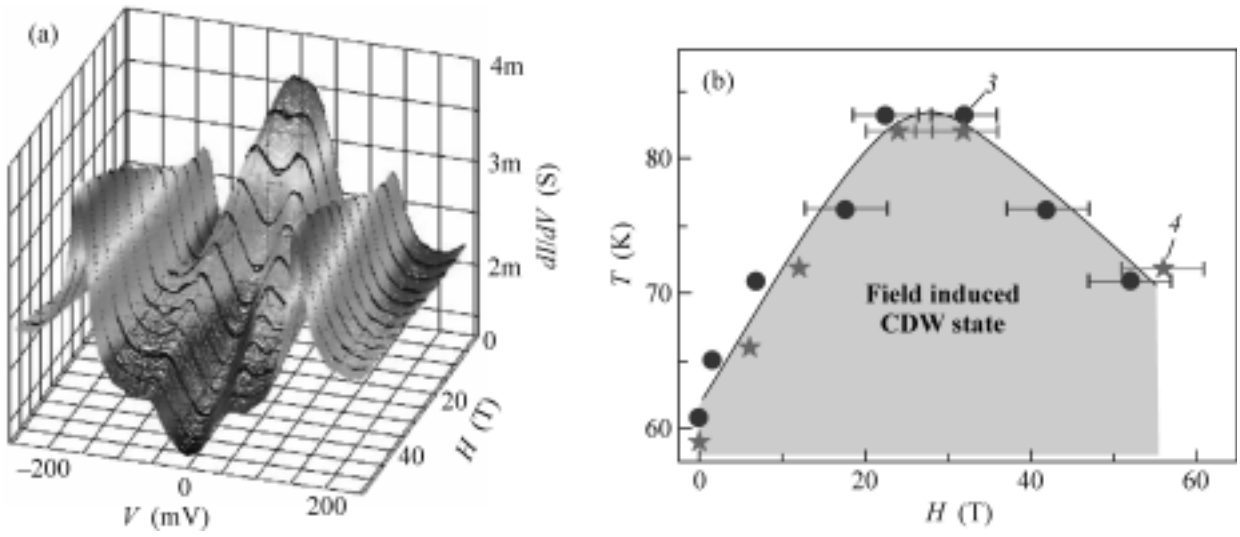

Fig. 1. (a) Three-dimensional diagram of tunnel spectra of the $NbSe_3$ mesa at various magnetic fields (**H** || **a*** at $T = 65$ K. (b) Field–temperature phase diagram of the field-induced charge density wave.

The experiments were carried out at the National Laboratory of Pulsed magnetic fields (Toulouse, France) with magnetic fields up to 55 T and a pulse duration of 300 ms. We developed a fast data-collection system at a frequency of 5 MHz that ensured the possibility of recording more than 1000 spectra per pulse. The magnetic-field-induced state with the charge density wave above T_p was actually detected. Figure 1a shows a series of tunnel spectra recorded at a fixed temperature by 5 K above T_{p2}. At zero magnetic field, gap features of the high-temperature charge density wave can be seen at $V = 140$ mV and gap features of the high-temperature charge density wave at $T > T_{p2}$ merge and form a wide maximum at zero bias. According to the figure, an increase in the field at $H \geq 3$ T is accompanied by the appearance of gap features, which indicate that the charge density wave energy gap appears under the action of the field. The amplitude of the gap feature of the high-temperature charge density wave increases with the field. Similar measurements at various temperatures can provide the phase diagram of the field-induced state with a charge density wave. This diagram is shown in Fig. 1b by the shaded (green on-line) region. The boundary of this region is the $T_p(H)$ dependence; it has a nonmonotonic character, which is similar to that predicted theoretically with a maximum at $H \approx 30$ T. An increase in T_p by 30% is achieved at the maximum. Since this effect is associated with the motion of uncondensed carriers in the plane of the layer, it should be the orbital effect. Indeed, comparative measurements in the perpendicular and parallel fields (Fig. 2) indicate that the effect exists only for the perpendicular orientation of the field. The presence of the maximum of $T_p(H)$ is attributed to the competition between the orbital effect and Pauli effect on the charge density wave energy gap. When the charge density wave is formed, electrons and holes with the total pulse $2p_F$ with parallel or antiparallel spins are paired. In zero field, the charge density wave state is degenerate with respect to the orientation of the spins. With an increase in the field, the subband with spins oriented along the field is shifted towards higher energies, which corresponds to an increase in k_F for this subband, whereas the subband with antiparallel spins is shifted towards lower energies and the corresponding k_F value decreases. This leads to the destruction of the initial state with a charge density wave with a wavevector of $2k_F$ and, correspondingly, to a decrease in T_p in fairly high fields. According to our experiments, the Zeeman splitting effect begins to dominate in fields higher than 30 T, which corresponds to the condition $2\mu_B H > 60$ K. A temperature of 60 K corresponds to the energy kT_p of the phase ordering of the charge density wave across the chains. Thus, the suppression of the field-induced stimulation of the charge density wave begins under the condition $2\mu_B H > kT_p$ or $H > kT_p/(2\mu_B H)$, which is very close to the numerical calculation reported in [11].

To summarize, we have revealed the stimulation of the charge density wave energy gap above the low Peierls transition temperature and showed the orbital character of this effect. The magnetic field dependence of the Peierls transition temperature has been determined from measurements. It has been shown that the effect is limited by the Zeeman splitting of the ground state.

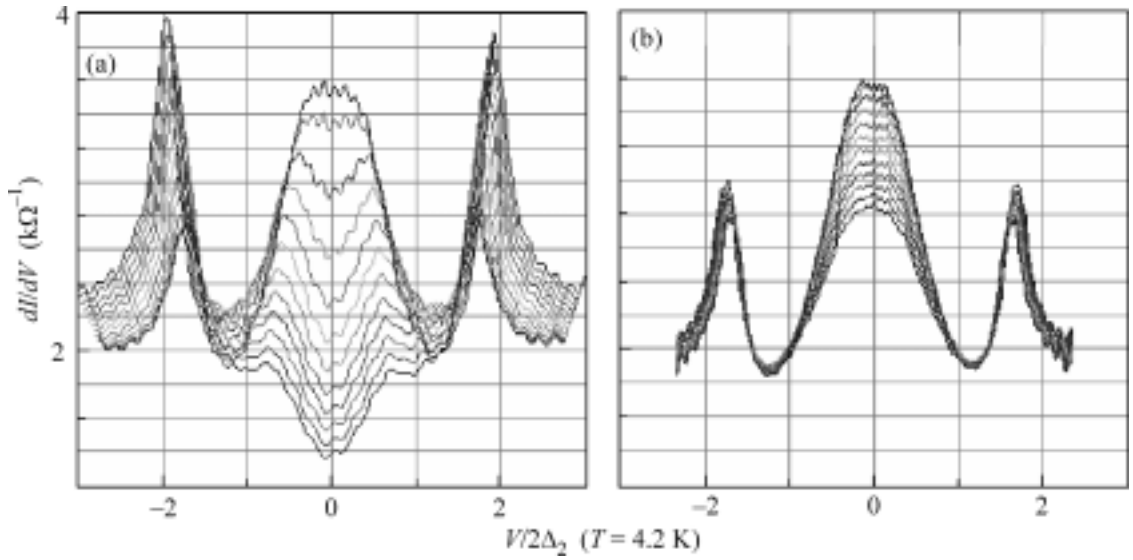

Fig. 2. Tunnel spectra for the magnetic fields (from top to bottom) 0, 4.9, 9.8, 14.7, 19.7, 24.4, 29.3, 34.4, 39.1, 44, 48.9, and 53.7 T (a) transverse and (b) parallel to the layers.

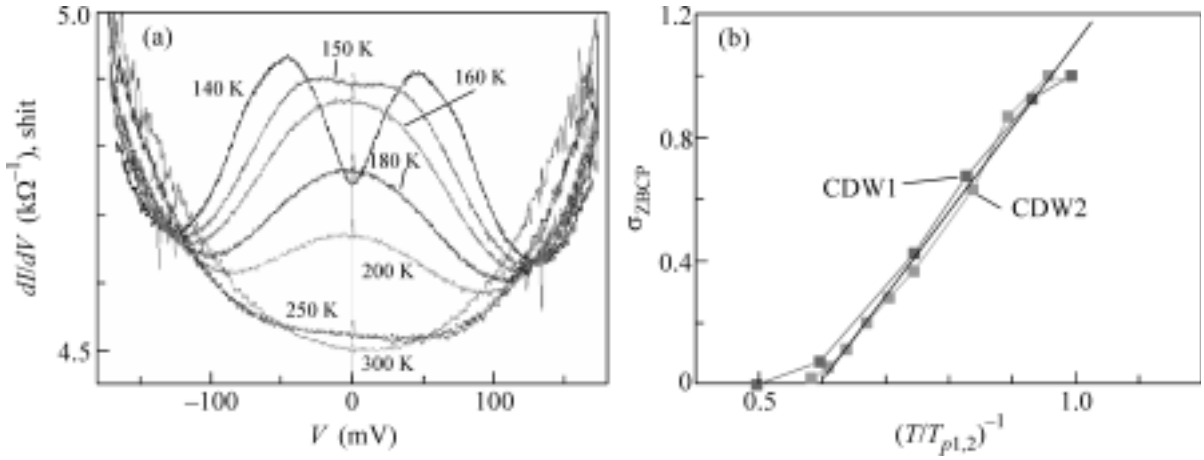

Fig. 3. (a) Interlayer tunnel spectra of $NbSe_3$ in the temperature range of 140–300 K. (b) Temperature dependence of the conductivity σ_{ZBCP} at zero bias divided by its value at $T = T_p$.

2.2. Spectroscopy of the Peierls State above the Transition Temperature

As was mentioned above, the gap feature of the density of states above T_p merge and form a wide maximum. This maximum determines the excess density of states at the Fermi level in the fluctuation region. We examined the temperature evolution of this maximum above T_{p1} (Fig. 3a). Evolution is observed up to very high temperatures (~250 K), which is twice as high as T_1 [7]. This result is in agreement with the X-ray diffraction data [12], according to which fluctuations in the charge density wave in $NbSe_3$ were observed at temperatures 150 K higher than T_{p1}. A similar fluctuation peak is also observed above the low-temperature Peierls transition temperature. It was shown that the height of the peak divided by its value at T_p and σ_{ZBCP} is a universal function of the reduced temperature T/T_p. For both charge density waves, $\sigma_{ZBCP} \propto (T/T_p)^{-1}$ (Fig. 3b), which indicates the universality of the behavior of the density of states in the fluctuation region.

2.3. Second Harmonic of the Gap Feature in $NbSe_3$

A detailed analysis of interlayer tunnel spectra in the high-temperature superconductor $Bi_2Sr_2CaCu_2O_{8+x}$ indicates not only the main gap feature at the bias $V = 2\Delta/e$, but also weak harmonic features at biases

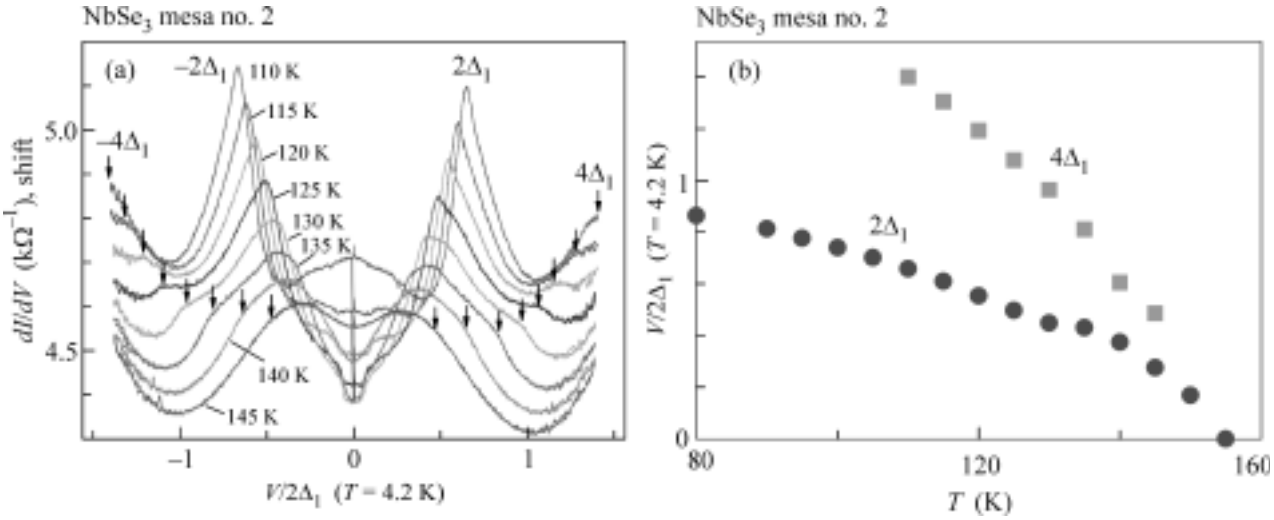

Fig. 4. (a) Interlayer tunnel spectra of $NbSe_3$ in the temperature range of 110–145 K. Arrows mark features at the bias voltage $V = 4\Delta/e$. (b) Temperature dependences of the gap peak at $V = 2\Delta/e$ and feature at $V = 4\Delta/e$.

$V = n \cdot 2\Delta/e$ for $n = 2, 3, \ldots$ [13]. This effect was explained by the fact that the tunneling of a quasiparticle with an excess energy in the transition at biases $V > 2\Delta$ is simplified if the quasiparticle transfers this energy to a phonon (or to a photon) because of the high density of empty states near the edge of the gap. Since the system contains many phonons with an energy of 2Δ due to recombination processes, the tunneling probability increases for quasiparticles with an excess energy of 2Δ. When the excess energy of the quasiparticle is 4Δ, similar two-photon processes are possible, etc.

Similar processes can be expected in the case of tunneling in the system with a charge density wave with a gap in the excitation spectrum and with the divergence of the density of states near the edge of the gap. We conducted a detailed analysis of the interlayer tunneling spectra in $NbSe_3$ near the upper Peierls transition that revealed these features (Fig. 4).

3. COHERENT EFFECTS IN LAYERED HIGH-TEMPERATURE SUPERCONDUCTORS

Layered high-temperature superconductors are specific because of the presence of two-dimensional superconducting layers that are separated by insulating layers and connected by the Josephson interaction. This medium can be considered as a sequence of interlayer Josephson junctions the behavior of which is also determined by the two-dimensional character of superconductivity in the layers. In the magnetic field transverse to the layers, vortex filaments of plane (two-dimensional) Abrikosov vortices appear, which are structured into a filament in different layers due to the magnetic and Josephson interaction [14]. Since these interactions are weak, the Abrikosov vortex filament in layered high-temperature superconductors is soft. Josephson vortices with the centers in the insulating layers appear in this system in the parallel field [15]. Since the motion of this vortex is not required, the destruction of superconductivity in the core region unlike the case of Abrikosov vortices, Josephson vortices can move very rapidly. As a result, interest in these vortices has increased because of their potential applications in fast electronics. Below, we consider two effects caused by the interaction between these different types of vortices in layered high-temperature superconductors.

3.1. Test of the Interaction between Vortex Filaments and Josephson Vortices through Column-Like Defects

Vortices of the same type, Abrikosov or Josephson, repulse each other. Abrikosov vortex filaments are attracted to Josephson vortices and tend to intersect them [16]. This circumstance was used to visualize Josephson vortices by Abrikosov vortex filaments [17]. It was theoretically shown that Abrikosov vortex filaments at the intersection point are locally polarized by superconducting currents circulating around a Josephson vortex (Fig. 5a) [18]. This polarization can be considered as a measure of the attraction of vortices. The characteristic length of local polarization in the plane of the layers is about λ_{ab} [16, 18]. We proposed and implemented the experimental test of this mechanism by introducing column defects in the direction of the c axis [19]. In the first approximation, the column defect can be considered as a hollow cylinder with a diameter of D that is smaller than λ_{ab} by a factor of 30 and is larger than the size of the vortex core ξ by a factor of 2–3. For this reason, the column defect is the efficient pinning center for the Abrikosov vortex

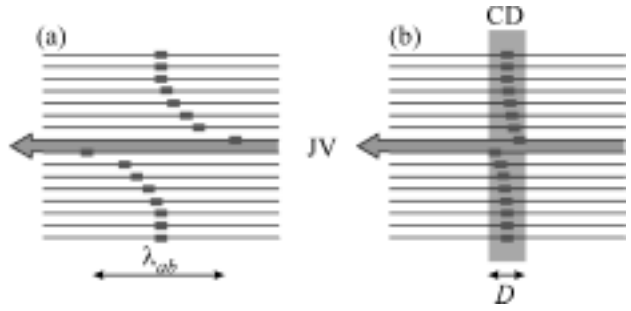

Fig. 5. Schematic of the Abrikosov vortex filament and (JV) Josephson vortex (a) at the point of their intersection and (b) under the pinning of the Abrikosov vortex filament on (CD) column-like defect.

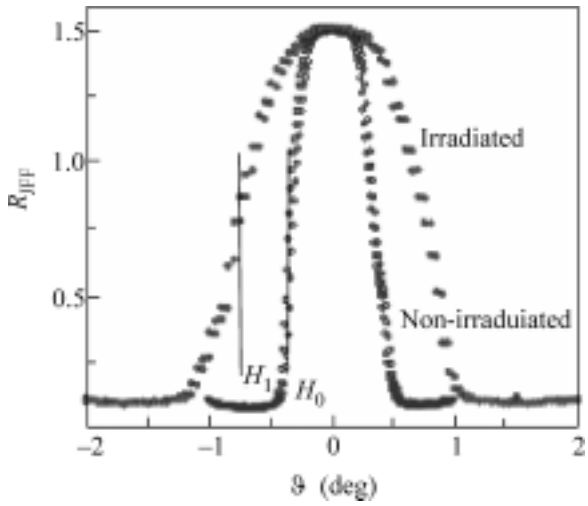

Fig. 6. Angular dependence of the reference in the regime of the motion of the lattice of Josephson vortices in the Bi-2212 mesa (lower points, blue in on-line version) before and (upper points, red in on-line version) after the introduction of column-like defects. Zero angle corresponds to the magnetic field parallel to the *a* axis $H_{||} = 1$ T. The transverse field component is $H_{||}\sin\vartheta$. The vertical lines mark the sharpest fall in the corresponding angular dependences $R_{JFF}(\vartheta)$ for the parameters $I = 60$ μA and $T = 45$ K. The concentration of the column-like defects is $c = 3 \times 10^8$ cm^{-2}.

filament. The polarization of the Abrikosov vortex filament in the column-like defect is strongly limited (Fig. 5b) and, correspondingly, the interaction between the Abrikosov vortex filament and Josephson vortex should be strongly suppressed. This interaction was experimentally studied in the regime of the sliding of the lattice of Josephson vortices on mesa-type structures. At a given current, the voltage on the mesa V_{Jff} is proportional to the velocity if the lattice of Josephson vortices. The appearance of Abrikosov vortex filaments in the system, which interact with Josephson vortices, strongly reduces the velocity if the lattice of Josephson vortices, which leads to a decrease in the voltage. Figure 6 shows the dependence of the voltage V_{Jff} (or the resistance R_{Jff} at a given current) on the deviation angle from the parallel orientation of the field, which is proportional to the transverse component of the field at small angles. The lower points (blue in the on-line version) correspond to the sample without column-like defects. The sharp decrease occurs at angles corresponding to the fields H_{c1} of the introduction of Abrikosov vortex filaments marked as H_0 in Fig. 6. The upper points (red in the on-line version) correspond to the sample after the introduction of column-like defects. The concentration of defects c was 3×10^8 cm^{-2} and corresponded to the equivalent field $H_e = c\Phi_0 = 62$ Oe. As can be seen, the introduction of defects does not affect the velocity of the lattice of Josephson vortices because the resistance at zero angle (exactly parallel orientation of the field) changes only slightly. The most important result is that a decrease in the $R_{Jff}(\vartheta)$ dependence in the case of the introduction of column-like defects occurs at angles corresponding to the fields at which all column-like defects are filled with vortex filaments, $H_1 = H_0 + H_e$. This means that, in fields $H_0 < H < H_1$, when an increase in the field is accompanied by the filling of column-like defects by Abrikosov vortex filaments, they slightly moderate the lattice of Josephson vortices because their polarizability is strongly suppressed by the boundaries of the column-like defect. All column-like defects are filled when the field reaches H_1. For this reason, with a further increase in the field, the formation of Abrikosov vortex filaments between column-like defects begins. Their polarization is not limited by defects; for this reason, the strong interaction with Josephson vortices appears, decelerates the lattice, and strongly reduces the resistance. The experiments under consideration clearly indicate that the interaction of the Josephson vortex with an Abrikosov vortex filament is determined by the polarization [19].

3.2. Coherent High-Frequency Response of Interlayer Josephson Junctions in Weak Transverse Fields

We also studied the interaction between two types of vortices under the conditions of a high-frequency subterahertz pump. The response of the current–voltage characteristics of mesa-type structures to the high-frequency field in the presence of the transverse magnetic field was experimentally studied. It was shown that the magnetic field is responsible for the coherent response of the Shapiro step-type in the current–voltage characteristics of mesas [20] (Fig. 7). The response is of a collective character because the position of each Shapiro step corresponds to the synchronization of all 100 elementary junctions of a mesa. The number of harmonics of the main Shapiro step increases with the radiation power. Unlike the response of the standard Josephson junction [21], where the amplitude of the

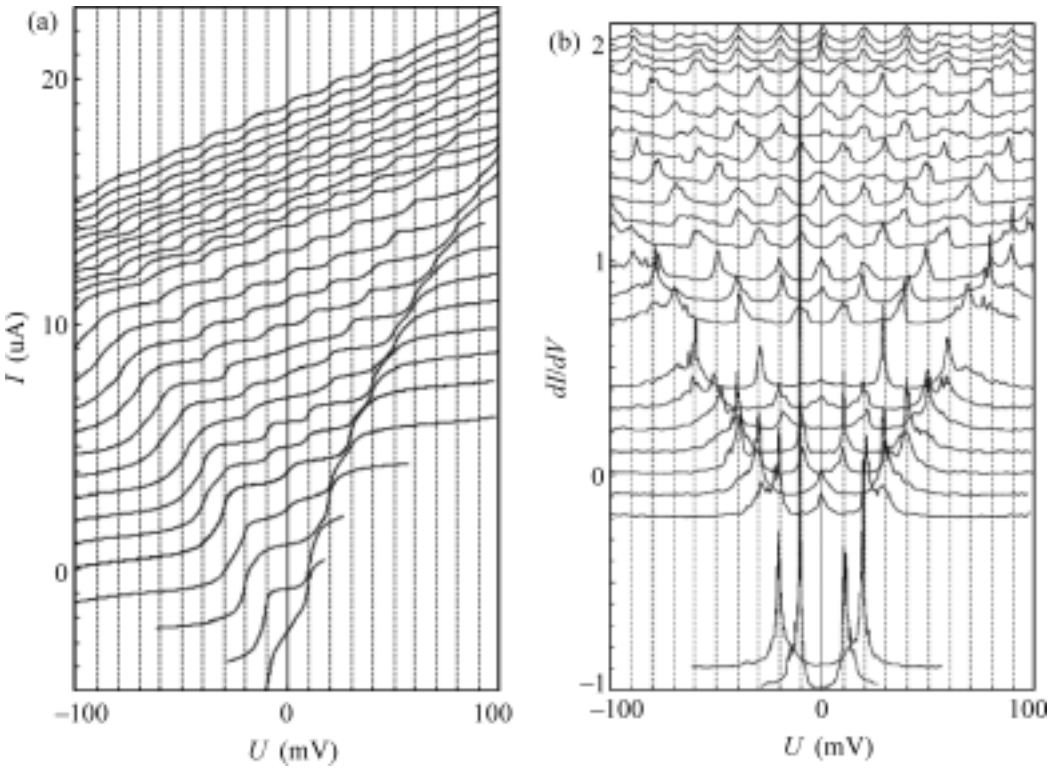

Fig. 7. (a) Current–voltage characteristics and (b) corresponding differential characteristics for the power referenced to 1 mW of 100-GHz external radiation (from bottom to top) −3.03, −1.15, 0.55, 2.23, 3.35, 4.41, 5.46, 6.36, 7.27, 8.17, 8.90, 9.63, 10.36, 10.93, 11.50, 12.07, 12.64, 12.88, 13.12, 13.44, 13.83, 14.23, 14.63, and 15.03 dBm. The curves were obtained at $T = 5$ K and are shifted along the vertical axis.

harmonic step decreases with an increase in its number, the amplitude of the last observed step is maximal at a given radiation power. Its position in V is proportional to the square root of the incident radiation power.

The observed coherent response is qualitatively explained by the fact that, due to the appearance of the Abrikosov vortex filament, the transverse magnetic field creates a periodic potential for the motion of Josephson vortices under the action of direct and high-frequency current [20]. In this case, the maximum response frequency is determined by the number of wells passed by the Josephson vortex in the period of variation of the high-frequency field. It is specified by the amplitude of the high-frequency current, i.e., is proportional to the root of the radiation power. Shapiro steps at lower frequencies are determined by the number of periods at which the vortex is displaced in a period of the high-frequency current in the sloping potential. Josephson vortices are created in the system by a weak parallel field and appear due to the entanglement of Abrikosov vortex filaments in magnetic fields close to the conditions of the melting of the vortex lattice.

Elementary junctions synchronize because Abrikosov vortex filaments pass through all elementary junctions and create a common periodic potential for all junctions.

3.3. Possible Applications

We proposed to use the observed effect to manufacture frequency converters based on a layered structure with elementary Josephson junctions [22]. The frequency multiplication factor is determined by the number of potential wells of the periodic lattice Abrikosov vortices that are passed by the Josephson vortex in the period of the variation of the high-frequency current. We experimentally studied mesas that have lateral sizes of 2×2 μm and contain about 100 elementary junctions. A substrate with a mesa was placed on the surface of a small permanent magnet, which generated a magnetic field of 0.1–0.2 T across the layers. The frequency of the external pump was 100 GHz. At a pump power of about 10 mW, the boundary Shapiro step is located at a voltage of 100 mV (Fig. 6), which corresponds to a frequency of 1 THz, which is an order of magnitude higher than the pump frequency. In this case, the power transformation coefficient is estimated as 10^{-4}–10^{-3}. To increase the transformation efficiency, one can use periodic arrays of mesas, as well as mesas with a large number of elementary junctions. Investigations indicate that the transverse magnetic

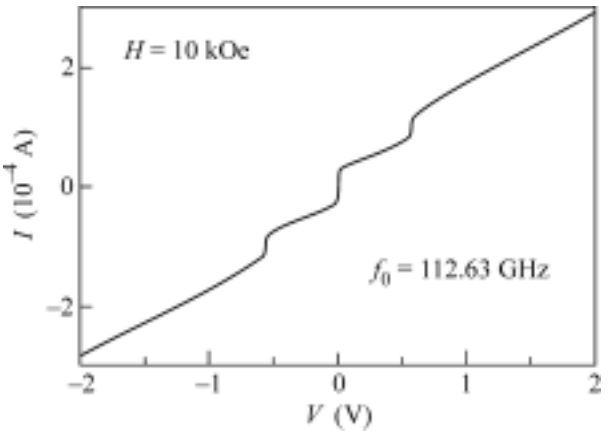

Fig. 8. Current–voltage characteristic of the Bi-2212 mesa irradiated by 112.63-GHz radiation in a transverse magnetic field of 1 T at $T = 20$ K.

field can synchronize at least 2500 elementary junctions [23] (Fig. 8). The corresponding Shapiro step under pumping by 113-GHz radiation is located at a voltage of about 0.6 V. These experiments indicate the possibility of creating a volt standard based on structures with the internal Josephson effect.

4. COHERENT EFFECTS IN GRAPHITE

The discovery of graphene and existence of massless carriers (Dirac fermions) refreshed an interest in graphite, particular in nanographite, which contains from several tens to several graphene layers. Scanning tunneling microscopy, magnetoabsorption, and Raman spectroscopy studies of thin graphite single crystals show that the surface layer of natural graphite is sometimes graphene on a graphite substrate. In this system, the scattering of Dirac fermions is even much smaller than in suspended graphene [24]. In this work, perforated graphite nanocrystals in which the surface transport is weakly shunted by the bulk of the sample [25] have been investigated for the first time.

4.1. Aharonov–Bohm Effect on Column-Like Defects in Ultrathin Graphite and Graphene

Samples with thicknesses of 50–1 nm (bigraphene) were obtained by flaking single crystals from natural graphite using adhesive tape, followed by the subsequent dissolution of the glue base of the tape in acetone and transfer of the sample on the substrate. Then, the sample was thinned to atomic thicknesses in a soft plasma of a beam–plasma reactor [26]. Nanoholes (antidots) oriented along the c axis were obtained in the samples by irradiation with either 90-MeV Xe ions (an antidot diameter of 24 nm) [25] or focused ion beams (a diameter of 35 nm). Due to the presence of antidots in both types of samples, there are oscillations of the magnetoresistance that are periodic in the field

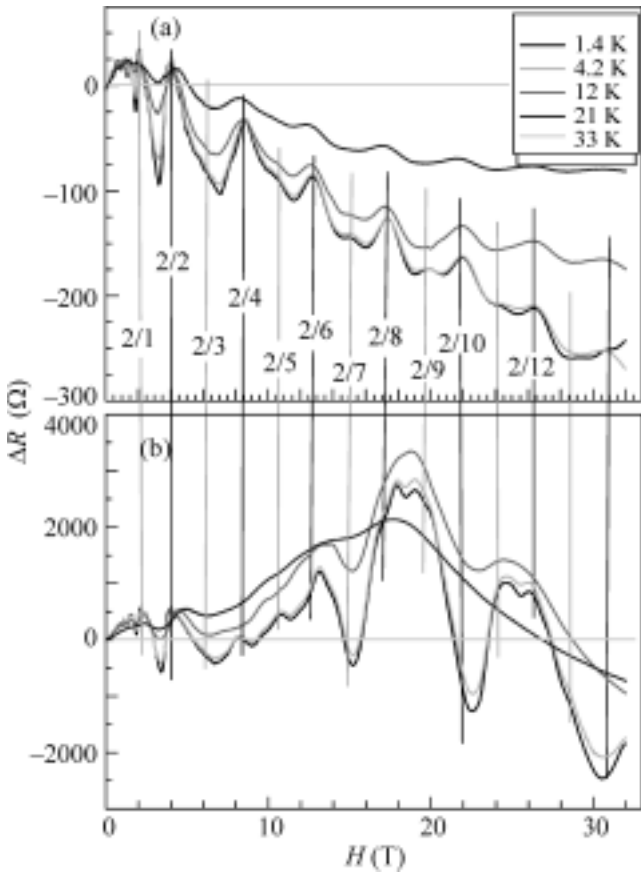

Fig. 9. Magnetoresistance of graphite single crystals with a thickness of (a) 50 and (b) 1 nm, which contain column-like defects 24 nm in diameter with a concentration of $c = 3 \times 10^9$ cm^{-2}. Arrows mark the minima and maxima of oscillations of the magnetoresistance. In both cases, the period of oscillations is 7.6 T.

($H \| c$) with the period in the flux corresponding to the flux quantum hc/e on the area of the antidot (Fig. 9a). These oscillations are particularly well seen in the ultraquantum limit in fields higher than 10 T, where Shubnikov–de Haas oscillations cease, and are manifested up to very high temperatures (≈50 K).

The period of oscillations corresponds to the interference of Dirac fermions under the condition that the main contribution comes from the orbits located near the edge of the antidot. This period is independent of the thickness of the sample down to 1 nm [27] (Figs. 9a, 9b), which indicates the decisive contribution from surface graphene.

We attribute the observation of the Aharonov–Bohm effect in samples of nonring geometry to the manifestation of the Tamm-type edge states, where carriers rotate around the antidot as in a ring and in the antidot, even in the absence of a magnetic field. If these states were disregarded, the interference of normal magnetic edge states that correspond to different orbits hopping around the antidot would strongly sup-

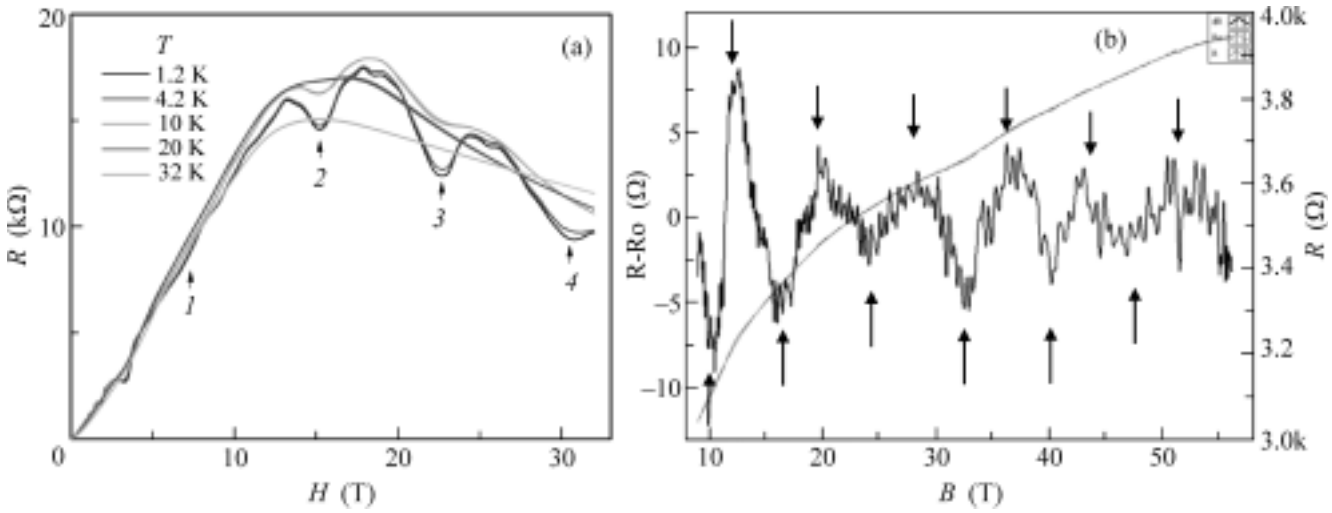

Fig. 10. Oscillating part of the magnetoresistance of natural graphite single crystals with a thickness of 50 nm, $\Delta R = R(H)_T - R(H)_{33\ \mathrm{K}}$ at temperatures $T = 1.4$–33 K for the (a) pure sample and (b) sample with column-like defects with a concentration of $c = 3 \times 10^9\ \mathrm{cm}^{-2}$ (see Fig. 9a). Vertical straight lines correspond to the maxima of $\Delta R(H)$ for the pure sample that correspond to the condition $H_n = H_0\nu$, where $H_0 = 4.4$ T, $\nu = 2/n$, and $n = 1, 2, 3, \ldots$.

press the effect. The theory of these edge states in graphene was developed for half-plane [28] and recently for the antidot [29]. According to [28], edge states are characterized by the linear spectrum with the velocity much lower than the Fermi velocity. The predictions of the theory are in agreement with the results of the observation of oscillations on structures with a single antidot. The experimentally determined velocity of carriers in the edge states is indeed an order of magnitude lower than the Fermi value [30].

4.2. Fine Structure of Oscillations of the Magnetoresistance

When examining the magnetoresistance of thin graphite samples without antidots, we revealed a fine field-periodic structure of the magnetoresistance. It is shown in Fig. 10a with the subtraction of the nonoscillating background of the magnetoresistance that is taken as the magnetoresistance at a temperature of 33 K. It is remarkable that this structure is also manifested in samples with a small number of column-like defects (Fig. 10b), where it is additively imposed on the Aharonov–Bohm oscillations, which were considered above. In fields higher than 4 T, the structure is manifested as a series of peaks in magnetic fields given by the expression

$$H_n = H_0/(2/n), \qquad (1)$$

where $H_0 = 4.4$ T and n is an integer. The quantity $1/H_0$ corresponds to the period of Shubnikov–de Haas oscillations for the dominant electron subsystem in graphite at $H < H_0$ [31, 32]. Consequently, the quantity $\nu = 2/n$ at $n > 2$ can be considered as the fractional filling factor of the ground Landau level.

In [33], on pyrolytic graphite samples, plateau features were also observed on the $R_{xy}(H)$ curve under condition (1) and $H > 17$ T. These features were attributed in [33] to the existence of interacting pairs of electrons (charged bosons [34]) for which the hierarchy of states in the fractional quantum Hall effect regime is described by the condition $\nu = 2/n$ [34]. The existence of charged bosons in graphite is yet insufficiently justified. The search for alternative explanations requires further investigations of these features, in particular on graphite samples with various thicknesses and in inclined fields.

Note that comparatively thick 0.5-mm graphite samples were examined in [33]. On our 50–100-nm samples, the effect is more pronounced. This may indicate that this effect is attributed to the surface of graphite, i.e., with Dirac fermions, as in the case of the observed Aharonov–Bohm oscillations.

5. CONCLUSIONS

Coherent phenomena in various layered materials in the presence of transport both along and across the layers have been examined. The stimulation of the charge density wave energy gap above the Peierls transition temperature in $NbSe_3$ has been revealed. The synchronization of the response of elementary Josephson junctions on $Bi_2Sr_2CaCu_2O_{8+x}$ mesostructures to subterahertz radiation under the action of the transverse magnetic field. On thin graphite and graphene samples with column-like defects, the Aharonov–Bohm effect has been revealed, which is due to

the contribution from Dirac fermions and indicates the existence of edge states around a nanohole.

This work was supported by the Russian Foundation for Basic Research (project nos. 08-02-01093a, 11-02-01379a, 11-02-90515-Ukr_f_a, and 11-02-12167-ofi-m), the Ministry of Education and Science of the Russian Federation (state contract nos. 16.740.11.0146, 02.740.11.0795, and 16.513.11.3066), the Russian Academy of Sciences, and Seventh Framework Program "Transnational Access," European Union (contract no. 228 043-Euromagnet II-Integrated Activities).

REFERENCES

1. Yu. I. Latyshev, P. Monceau, A. A. Sinchenko, et al., J. Phys. A: Math. Gen. **36**, 9323 (2003).
2. Yu. I. Latyshev, P. Monceau, S. A. Brazovskii, et al., J. Phys. (Fr.) IV **131**, 197 (2005).
3. A. P. Orlov, Yu. I. Latyshev, A. M. Smolovich, et al., JETP Lett. **84**, 89 (2006).
4. Yu. I. Latyshev, P. Monceau, S. Brazovskii, et al., Phys. Rev. Lett. **95**, 266402 (2005).
5. Yu. I. Latyshev, P. Monceau, S. Brazovski, et al., Phys. Rev. Lett. **96**, 116402 (2006).
6. A. P. Orlov, Yu. I. Latyshev, D. Vingnolles, et al., JETP Lett. **87**, 433 (2008).
7. Yu. I. Latyshev, A. P. Orlov, A. Yu. Latyshev, et al., Physica B **404**, 399 (2009).
8. C. A. Balseiro and L. M. Falicov, Phys. Rev. Lett. **55**, 2336 (1985).
9. R. V. Coleman, G. Eiserman, M. P. Everson, et al., Phys. Rev. Lett. **55**, 863 (1985).
10. L. P. Gor'kov and A. G. Lebed, J. Phys. Lett. **45**, 433 (1984).
11. D. Zanchi, A. Bjelis, and G. Montabaux, Phys. Rev. B **53**, 1240 (1996).
12. J. P. Pouget, R. Moret, A. Meerschaut, et al., J. Phys. C3 **44**, 1729 (1983).
13. V. M. Krasnov, Phys. Rev. Lett. **97**, 257003 (2006); cond-mat. arXiv:0910.0161.v1.
14. S. N. Artemenko and A. N. Kruglov, Phys. Lett. A **143**, 485 (1990); A. I. Buzdin and D. Feinberg, J. Phys. (Paris) **51**, 1971 (1990).
15. J. R. Clem and M. W. Coffey, Phys. Rev. B **42**, 6209 (1990).
16. A. E. Koshelev, Phys. Rev. Lett. **83**, 187 (1999).
17. A. N. Grigorenko, S. Bending, T. Tamegai, et al., Nature **414**, 728 (2001).
18. M. J. W. Dodgson, Physica C **369**, 182 (2002).
19. Yu. I. Latyshev, M. Konczykowski, and S.-J. Kim, JETP Lett. **89**, 402 (2009).
20. V. N. Pavlenko, Yu. I. Latyshev, J. Chen, et al., JETP Lett. **89**, 291 (2009).
21. A. Barone and G. Paterno, *Physics and Applications of the Josephson Effect* (Wiley, New York, 1982).
22. Yu. I. Latyshev, J. Chen, and M. B. Gaifullin, in *Proceedings of the 7th International Symposium on Intrinsic Josephson Effects and Plasma Oscillations in High-T_c Superconductors, Apr. 29–May 2, 2010* (Hirosaki, Aomori, Japan, 2010), p. 38.
23. M. B. Gaifullin, K. Hirata, S. Ooi, et al., Physica C **468**, 1896 (2008).
24. P. Nuegebauer, M. Orlita, C. Faugeras, et al. Phys. Rev. Lett. **103**, 136403 (2009).
25. Yu. I. Latyshev, A. Yu. Latyshev, A. P. Orlov, et al., JETP Lett. **90**, 480 (2009).
26. V. A. Bykov, Yu. I. Latyshev, E. G. Shustin, et al., RF Patent No. 2413330 (2011).
27. Yu. I. Latyshev, A. P. Orlov, E. G. Shustin, et al., J. Phys.: Conf. Ser. **248**, 012001 (2010).
28. V. A. Volkov and I. V. Zagorodnev, J. Phys.: Conf. Ser. **193**, 012113 (2009).
29. Yu. I. Latyshev, A. P. Orlov, V. A. Volkov, et al., in *Proceedings of the Conference on Strong Correlated Electron Systems and Quantum Critical Phenomena, June 18, 2010* (Troitsk, 2010), p. 12.
30. Yu. I. Latyshev, A. P. Orlov, P. Monso, and V. Eskoffier, in *Proceedings of the 15th International Symposium on Nanophysics and Nanoelectronics, March 14–18, 2011* (Nizhni Novgorod, 2011), Vol. 1, p. 111.
31. I. A. Luk'yanchuk and Y. Kopelevich, Phys. Rev. Lett. **97**, 256801 (2006).
32. J. V. Scneider, M. Orlita, M. Potemski, et al., Phys. Rev. Lett. **102**, 166403 (2009).
33. Y. Kopelevich, B. Raquet, M. Goiran, et al., Phys. Rev. Lett. **103**, 116802 (2009).
34. B. I. Halperin, Helv. Phys. Acta **56**, 75 (1983).

Translated by R. Tyapaev

SPELL: OK